



Numerical conformal mapping methods based on Faber series

Thomas K. DeLillo^{a,*,1,2}, Alan R. Elcrat^{a,2}, John A. Pfaltzgraff^b

^a *Department of Mathematics and Statistics, Wichita State University, Wichita, KS 67260-0033, USA*

^b *Department of Mathematics, The University of North Carolina at Chapel Hill, CB 3250, Phillips Hall, Chapel Hill, NC 27599-3250, USA*

Abstract

Methods are presented for approximating the conformal map from the interior of various regions to the interior of simply-connected target regions with a smooth boundary. The methods for the disk due to Fornberg (1980) and the ellipse due to DeLillo and Elcrat (1993) are reformulated so that they may be extended to other new computational regions. The case of a cross-shaped region is introduced and developed. These methods are used to circumvent the severe ill-conditioning due to the crowding phenomenon suffered by conformal maps from the unit disk to target regions with elongated sections while preserving the fast Fourier methods available on the disk. The methods are based on expanding the mapping function in the Faber series for the regions. All of these methods proceed by approximating the boundary correspondence of the map with a Newton-like iteration. At each Newton step, a system of linear equations is solved using the conjugate gradient method. The matrix–vector multiplication in this inner iteration can be implemented with fast Fourier transforms at a cost of $O(N \log N)$. It is shown that the linear systems are discretizations of the identity plus a compact operator and so the conjugate gradient method converges superlinearly. Several computational examples are given along with a discussion of the accuracy of the methods.

Keywords: Numerical conformal mapping; Faber series; Fornberg's methods; Crowding

AMS classification: 30C30; 65E05

1. Introduction

Numerical conformal mapping has been an active area of research in recent years. The books by Gaier [15] and Henrici [18] give an introduction to the wide variety of methods that have been developed. Several such methods seek to construct the conformal map from the unit disk to a simply-connected target region by essentially representing the mapping function by a truncated Taylor series. Using the unit disk as a computational domain is attractive since it permits the use

* Corresponding author. E-mail: delillo@twsvum.uc.twsu.edu.

¹ Research was partially supported by U.S. Department of Energy grant DE-FG02-92ER25124.

² Research was partially supported by National Science Foundation EP-SCoR Grant OSR-9255223.

of Fourier series and the fast Fourier transform (FFT) algorithm. Presentations of several algorithms along with numerical examples are given in [4, 5, 14, 24, 25, 27].

Unfortunately, conformal maps may suffer from severe distortions. The conformal map from the unit disk to a simply-connected region with elongated sections has distortions that may vary exponentially with the aspect ratio of the elongated section. This severe ill-conditioning, known as the crowding phenomenon, limits the usefulness of numerical conformal mapping methods from the unit disk by requiring the use of an impractically large number of terms in the Taylor series. These limitations are especially inconvenient in applications; see [7, 14]. Regions with “pinched” sections exhibit somewhat less severe distortions which may vary algebraically with the thinness of the pinched section. For estimates of the crowding and a number of examples and references to the literature, see [4, 10, 31].

In recent years, various numerical methods have been developed which avoid the crowding problem in certain cases. In Howell and Trefethen [20], the crowding for the Schwarz–Christoffel map for elongated polygons is discussed. There a method which uses the infinite strip for the computational domain instead of the unit disk is developed. The domain decomposition methods of Papamichael and Stylianopoulos (see [22] and references therein) can be used to map more general elongated regions onto elongated rectangles. Applications include calculations of resistance of semiconductor circuits. A very recent, new method by Driscoll and Vavasis [12] handles the crowding of the prevertices in the Schwarz–Christoffel transformation for elongated polygons by instead using certain cross-ratios as the primitive variables.

The present paper is a continuation of efforts [6] to circumvent the crowding for regions with smooth boundaries by choosing computational domains with elongated sections. Roughly speaking, we approximate the conformal map from the computational region in the z -plane to the target region by a finite Faber series,

$$f(z) = A_0 + \sum_{m=1}^{N/2} A_m F_m(z),$$

where $F_m(z)$ is the m th degree Faber polynomial of the computational region and A_m is the m th Faber coefficient. For the disk, $F_m(z) = z^m$. If the target region is elongated in one direction an ellipse of similar minor-to-major axis ratio is an appropriate computational domain. For the ellipse, $F_m(z)$ is just the m th degree Chebyshev polynomial. To illustrate the advantage of our methods, consider the cigar-shaped target region given by the arctanh function of example 2, Section 5; see Fig. 1, top two maps. If the minor-to-major axis ratio is $\alpha = 0.29$ ($r = 0.99$), the map from the unit disk required $N = 1024$ and 6.8 CPU seconds to achieve an accuracy of $0.4 \cdot 10^{-5}$, whereas the map from an ellipse of minor-to-major axis ratio $\alpha = 0.3$ to the arctanh region required only $N = 64$ and 1.1 CPU seconds to achieve an accuracy of $0.2 \cdot 10^{-6}$. Moreover, much more elongated regions can be mapped using ellipses of similar minor-to-major axis ratio. For four-legged regions the Faber series for a cross-like region is used; see Fig. 1, bottom two maps. Other geometries, such as multi-legged or exterior domains for which the Faber series are known, are also possible.

Our numerical approach is an extension of Fornberg’s method [14] for the disk and proceeds by approximating the boundary correspondence of the map with a Newton-like iteration. Conditions that the mapping f is analytic are transplanted to an annulus with an explicit map, ψ , as illustrated in Figs. 7 and 8 and discussed in Section 3. The resulting conditions on the Laurent coefficients of the

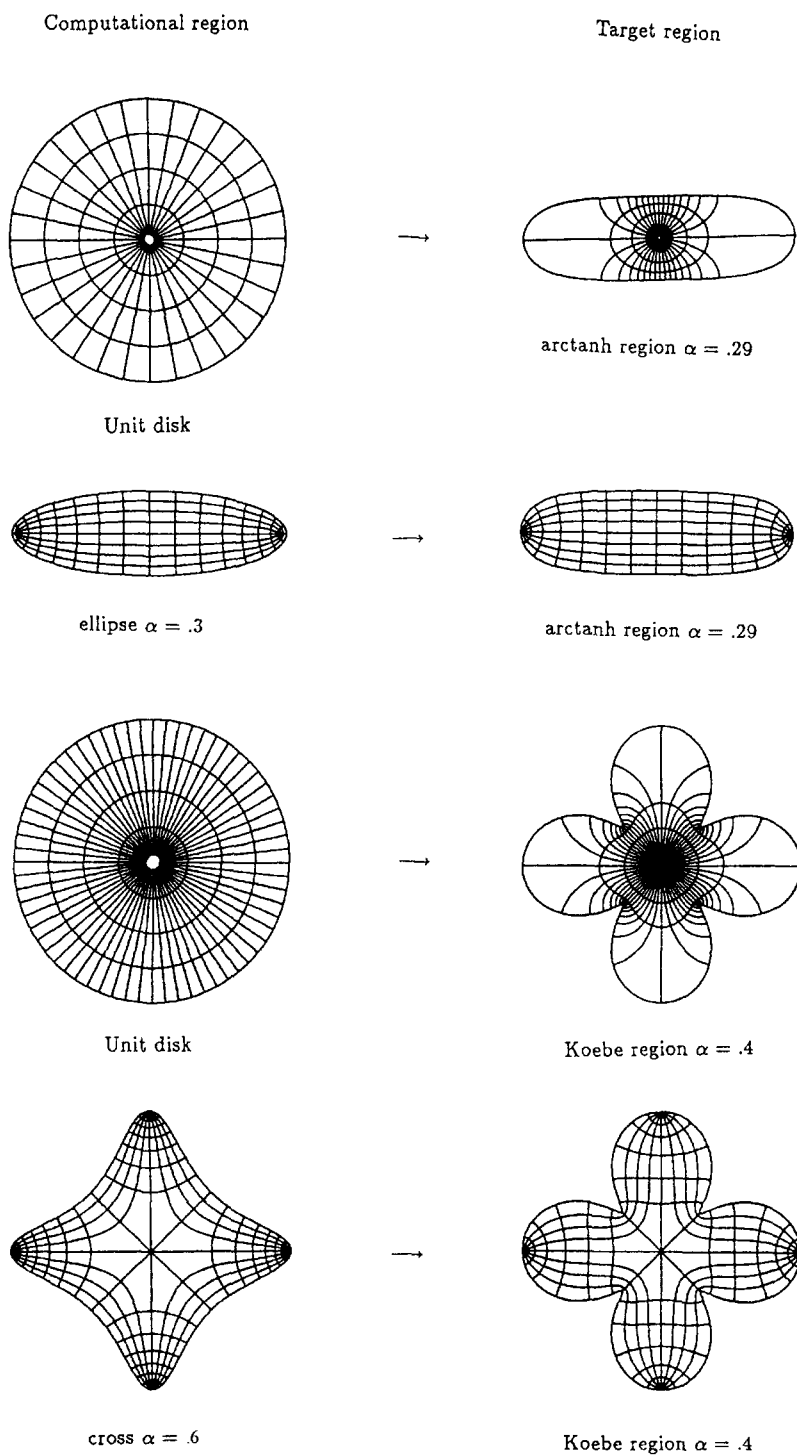


Fig. 1. Top two maps: arctanh region $\alpha = 0.29$ with disk map with $N = 1024$ and ellipse map with $\alpha_{\text{ellipse}} = 0.3, N = 64$. Bottom two maps: 4-leaf Koebe region $\alpha = 0.4$ with disk map with $N = 1024$ and cross map with $\alpha_{\text{cross}} = 0.6, N = 256$.

transplanted function give a system of linear equations for the Newton update of the boundary correspondence. This system is solved by the conjugate gradient method. The matrix–vector multiplication can be performed in $O(N \log N)$ using FFTs. We have reformulated the original methods for the disk [14] and the ellipse [6] here, so that they extend in a straightforward way to new geometries. We also show how to revise our methods so that 3 boundary points can be fixed (Figs. 4 and 6), instead of 1 boundary point and an interior point as in [6].

Our basic idea of combining analyticity conditions for the computational region with extensions of Fornberg’s method to yield a Newton-like method has been generalized to multiply connected regions [11, 9]. These multiply connected cases give a Newton iteration for finding both the boundary correspondences and the conformal moduli.

Applications of these methods include computational problems in potential theory. For instance, it is well known that the Dirichlet problem can be conformally transplanted to the disk and solved efficiently with FFTs. Similar formulas are available for the ellipse [18, p. 231, Problem 3] and the cross. Calculations currently under way demonstrate that this procedure compares favorably with integral equation methods for elongated regions [8]. In addition, Muskhelishvili’s method for solving the biharmonic equation using conformal mapping from the disk [1] can be extended to the ellipse case.

The paper is organized as follows. In Section 2, we state some known preliminary results that will be used in our later development. In Section 3, we derive the linearized equations for the disk, ellipse, and cross method and show that they are equal to the identity plus a compact operator, so that conjugate-gradient-like methods are expected to converge superlinearly. In Section 4, discretization of the equations by trigonometric interpolation, the application of the normalization conditions, and the solution of the discrete equations by the conjugate gradient method are developed and discussed. The numerical evaluation of the mapping function is also explained. In Section 5, our methods are applied to several examples. Section 6 discusses the features of the methods which influence the accuracy of the numerical approximations.

2. Preliminaries

Suppose that f is a conformal map from the domain D in the z -plane, bounded by the Jordan curve C , to the domain Ω in the w -plane, bounded by the Jordan curve Γ . Assume that both D and Ω contain the origin. Suppose further that C is described by a function $z(\theta)$, $0 \leq \theta \leq 2\pi$, and Γ by $\gamma(S)$, S being arc length along Γ , and that z, γ are Hölder continuously differentiable with nonvanishing derivatives. The normalizations $f(0) = 0$ and $f(z(0)) = \gamma(0)$ uniquely determine f ; further, finding f is equivalent to finding the function $S(\theta)$ such that $f(z(\theta)) = \gamma(S(\theta))$. This function is called the *boundary correspondence*. Most methods for constructing f are methods for finding $S(\theta)$ (or its inverse); we will use a Newton-like method for the nonlinear singular integral equation

$$\frac{1}{2\pi} \int_C \frac{\gamma(S(\zeta))}{\zeta - z} d\zeta = \frac{1}{2} \gamma(S(z)), \quad z \in C,$$

for $S(z) = S(z(\theta)) = S(\theta)$. More precisely, if $S^{(k)}(\theta)$ is known we determine $U^{(k)}(\theta) = S^{(k+1)}(\theta) - S^{(k)}(\theta)$ by the condition that $\xi(\theta) + e^{i\beta(\theta)} U^{(k)}(\theta)$, where $\xi(\theta) := \gamma(S^{(k)}(\theta))$ and $\beta(\theta) := \arg \gamma'(S^{(k)}(\theta))$, extends into D as an analytic function continuous on $D \cup C$ which vanishes at the origin. This function is

a conformal map onto a neighboring domain $\tilde{\Omega}$. The function $S^{(k+1)}(\theta)$ is then taken to be the new approximation to the boundary correspondence; the boundary normalizations of the approximate maps are guaranteed by choosing $U^{(k)}(0) = 0$. Wegmann [24] has proven that this “equation” for U always has a unique solution, and that if the curves are twice Lipschitz continuously differentiable this iteration converges for an initial guess which is close enough in a Hölder norm.

If D is the unit disk, computing the Newton update is a problem in Fourier analysis. Fornberg [14] and Wegmann [24–29], have given (closely related) algorithms for solving this problem. In this work we will study a generalization of Fornberg’s work designed to deal with domains which are elongated in one or more directions. We assume our computational domain D is bounded by a curve C_ρ , and that C_ρ is the image under an analytic map ψ from a parameter plane, denoted by ζ , of the circle $|\zeta| = \rho > 1$. We further assume that ψ is a conformal map on $|\zeta| > 1$ fixing infinity and the positive direction. In particular, ψ is the normalized conformal map of $|\zeta| > \rho$ onto the exterior of C_ρ . Specific ψ ’s will be given below. We here emphasize the part of the framework that does not depend on detailed properties of ψ .

This work is based on a necessary and sufficient condition for a function f defined on C_ρ to extend into D as an analytic function. We recall the following fundamental fact [18, p. 114].

Proposition 1. *A Hölder continuous function f on C_ρ extends into D as an analytic function if and only if*

$$\int_{C_\rho} f(z)z^m dz = 0, \quad m \geq 0.$$

We will use the Faber polynomials $F_m(z)$ of degree m associated with D which can be defined [23], by the expansion

$$\frac{\zeta\psi'(\zeta)}{\psi(\zeta) - z} = \sum_{m=0}^{\infty} F_m(z)\zeta^{-m}, \quad z \in D, \quad |\zeta| > \rho.$$

We remark that z^m may be replaced by any polynomial of degree m in Proposition 1. In particular, we may replace z^m by $F_m(z)$. The basis of our method can then be described as follows: transplant the condition of Proposition 1 to the circle $|\zeta| = \rho$ and use Fourier series to implement this condition. If this is done, then, for f analytic in D , by Cauchy’s theorem

$$\begin{aligned} f(z) &= \frac{1}{2\pi i} \int_{C_\rho} \frac{f(\tilde{z})}{\tilde{z} - z} d\tilde{z} \\ &= \frac{1}{2\pi i} \int_{|\zeta|=\rho} \frac{f(\psi(\zeta))\psi'(\zeta)}{\psi(\zeta) - z} d\zeta \\ &= \frac{1}{2\pi i} \int_{|\zeta|=\rho} f(\psi(\zeta)) \sum_{m=0}^{\infty} F_m(z)\zeta^{-m-1} d\zeta \\ &= A_0 + \sum_{m=1}^{\infty} A_m F_m(z), \end{aligned}$$

where

$$A_m = \frac{1}{2\pi i} \int_{|\zeta|=\rho} f(\psi(\zeta)) \zeta^{-m-1} d\zeta$$

is the coefficient in the expansion of f in Faber polynomials in D . If f is analytic in a neighborhood of $|\zeta| = \rho$ and a_m are its Laurent coefficients then

$$A_m = \rho^{-m} a_m, \quad m \geq 0.$$

Implementation of this idea requires more detailed information about C_ρ and ψ . We will carry this out below in two cases: C_ρ is an ellipse and $\psi(\zeta) = \zeta + 1/\zeta$, and C_ρ is a symmetric “cross” shaped region with $\psi(\zeta) = \sqrt{\zeta^2 + 1/\zeta^2}$.

We conclude this section by collecting some known results from Fourier analysis and the theory of univalent functions.

We will need several operators occurring in Fourier analysis. The domain of these operators is the set of absolutely continuous 2π -periodic functions h with square integrable derivatives. We then write, as in [26],

$$P_- h = \frac{1}{2}(I - iK + J)h,$$

where K is the conjugation operator,

$$Kh(\theta) = \frac{1}{2\pi} P.V. \int_0^{2\pi} \cot\left(\frac{\theta - \phi}{2}\right) h(\phi) d\phi,$$

and

$$Jh(\theta) = \frac{1}{2\pi} \int_0^{2\pi} h(\theta) d\theta.$$

If

$$h(\theta) = \sum_{k=-\infty}^{\infty} a_k e^{ik\theta},$$

then

$$Kh(\theta) = i \sum_{k=-\infty}^{-1} a_k e^{ik\theta} - i \sum_{k=1}^{\infty} a_k e^{ik\theta},$$

$$Jh(\theta) = a_0,$$

and

$$P_- h(\theta) = \sum_{k=-\infty}^0 a_k e^{ik\theta}.$$

We will discretize these operators by N -point trigonometric interpolation. If

$$\mathbf{h} = (h(\theta_0), \dots, h(\theta_{N-1}))^T, \quad \theta_k = 2\pi k/N, \quad k = 0, \dots, N-1,$$

and

$$\hat{a}_k = \frac{1}{N} \sum_{j=0}^{N-1} h(\theta_j) w^{-jk}, \quad w = e^{2\pi i/N},$$

then the trigonometric polynomial interpolating h is given by

$$T_N h(\theta) = \sum_{k=-N/2+1}^{N/2-1} \hat{a}_k e^{ik\theta} + \hat{a}_{N/2} \cos\left(\frac{N}{2}\theta\right),$$

and the discrete operators corresponding to those introduced above are

$$K_N h(\theta) = i \sum_{k=-N/2+1}^{-1} \hat{a}_k e^{ik\theta} - i \sum_{k=1}^{N/2-1} \hat{a}_k e^{ik\theta},$$

$$J_N h(\theta) = \hat{a}_0 - \hat{a}_{N/2} \cos\left(\frac{N}{2}\theta\right),$$

and

$$P_{-,N} = \frac{1}{2}(T_N - iK_N + J_N).$$

If the $N \times N$ matrix $F := (w^{-kv})$, $k, v, = 0, \dots, N - 1$, then

$$\frac{1}{N} F^H F = I_N, \quad \frac{1}{N} F \mathbf{h} = \mathbf{a} = (\hat{a}_0, \dots, \hat{a}_{N-1})^T = (\hat{a}_0, \dots, \hat{a}_{N/2}, \hat{a}_{-N/2+1}, \dots, \hat{a}_{-1})^T,$$

since $\hat{a}_k = \hat{a}_{k-N}$, and

$$\frac{1}{N} P_{-,N} \mathbf{h} = \frac{1}{N} F^H \begin{pmatrix} I_1 & 0 \\ 0 & I_2 \end{pmatrix} F \mathbf{h},$$

where I_N is the $N \times N$ identity matrix, H denotes Hermitian conjugation, and I_1, I_2 are the $N/2 \times N/2$ matrices $\text{diag}(1, 0, \dots, 0)$ and $\text{diag}(0, 1, \dots, 1)$, respectively.

The following characterization of Faber polynomials can be found, for example, in [23].

Proposition 2. $F_m(z)$ is the unique m th degree polynomial such that

$$F_m(\psi(\zeta)) = \zeta^m + o(1) \quad \text{as } \zeta \rightarrow \infty.$$

We also need [17, p. 48],

Proposition 3. If k is a univalent function on $|\zeta| > 1$ fixing infinity, so is $\sqrt[m]{k(\zeta^m)}$ for $m > 1$.

3. Analyticity conditions and linear operator equations

We are concerned with the structure of the linearized equations arising at each step of the Newton's method for the boundary correspondence. This may be cast as a problem in Fourier analysis by

transplantation to the circle $|\zeta| = \rho$. In order to set the context, for what follows, we first describe the situation when D is the unit disk. The case in which D is an ellipse, a cross-shaped region, and some other possible extensions will then be considered. The *analyticity conditions* from Proposition 1, which guarantee that a function defined on the boundary of D extends analytically to the interior of D , will be derived in each case and shown to lead to linear operator equations for the Newton updates, $U(\theta)$. The linear operators will be seen to be roughly of the form identity plus a compact operator. Additional conditions, such as the normalization $f(0) = 0$, will be discussed here and in more detail in Section 4.

3.1. Disk

Our goal is to determine the conformal map from the unit disk D onto Ω normalized by $f(0) = 0$ and $f(1)$ fixed. The parameter domain is the ζ -plane with $\psi(\zeta) = \zeta$; the Faber polynomials are the powers, $F_m(z) = z^m$. For a function h defined on the unit circle C , h extends into D as an analytic function if and only if

$$\int_C h(z)z^m dz = \int_{|\zeta|=1} h(\zeta)\zeta^{m+1} d\zeta/\zeta = 0, \quad m = 0, 1, \dots,$$

that is, the negative indexed Fourier coefficients vanish, $a_m = 0, m > 0$. The normalization $h(0) = 0$ holds if and only if $a_0 = 0$. The power series of a function analytic inside a disk is its Faber series. The condition that $h = \xi + e^{i\beta}U$ extends into D as an analytic function vanishing at the origin is equivalent to $P_-h = 0$. Since U is real

$$(I + R)U = g,$$

where

$$RU = \text{Re}(e^{-i\beta}(J - iK)e^{i\beta}U),$$

and

$$g = -2\text{Re}(e^{-i\beta}P_- \xi).$$

Wegmann [26] and Widlund [30] have analysed Fornberg’s method [14] using the operator R , which can be represented as a Fredholm integral operator on $L^2(0, 2\pi)$ with kernel

$$R(\theta, \phi) = \frac{1}{2\pi} \sin(\beta(\phi) - \beta(\theta) + (\theta - \phi)/2) / \sin((\theta - \phi)/2).$$

This is a symmetric, compact operator. The eigenvalue distribution of R and its discretization is discussed in Section 4.1.

3.2. Ellipse

We begin our work on other computational domains with the ellipse. This case was dealt with recently in [6] using different normalizations and a different arrangement of the computations. In this case $\psi(\zeta) = \zeta + 1/\zeta$ and C_ρ is the image of $|\zeta| = \rho > 1$, that is the ellipse in the z -plane with

foci at ± 2 , and lengths of semi-major and semi-minor axes, $\rho + 1/\rho$, and $\rho - 1/\rho$, respectively. The mapping $w = f(z)$ will be normalized by $f(0) = 0$ and $f(\rho + 1/\rho)$ fixed at a point on $\Gamma : \gamma(S)$. We define $f(\theta) = f(\psi(\rho e^{i\theta})) = \gamma(S(\theta))$ where S is arc length on γ . We have here

$$F_m(z) = T_m(z) = 2^{-m}((z + \sqrt{z^2 - 4})^m + (z - \sqrt{z^2 - 4})^m),$$

that is, F_m is the Chebyshev polynomial of the first kind. Proposition 2 applies, since

$$F_m(\psi(\zeta)) = \zeta^m + \zeta^{-m}.$$

By Proposition 1, a function h is analytic inside C_ρ if and only if

$$\int_{C_\rho} h(z)T_m(z) dz = 0, \quad m \geq 0.$$

If we denote the functions transplanted to the ζ -plane with the same letter, this is equivalent to

$$\int_{|\zeta|=\rho} h(\zeta)(\zeta^m + \zeta^{-m})(\zeta - \zeta^{-1}) d\zeta/\zeta = 0;$$

in particular, if $h(\theta) = \sum_{m=-\infty}^{\infty} a_m e^{im\theta}$, this implies that

$$a_{-m} = \rho^{-2m} a_m, \quad m \geq 1, \tag{1}$$

as in [6]. This condition plays the role here that $P_-h = 0$, i.e. vanishing of negative index Fourier coefficients, does when D is the disk. We define the operator c by $c(e^{ik\theta}) = e^{-ik\theta}$, and let

$$l(\theta) = 1/(1 - \rho^{-2}e^{i\theta}).$$

Then (1) is equivalent to

$$(P_- - J - cl*)h = 0$$

where $*$ denotes convolution. This is applied to $h = \xi + e^{i\beta}U$ to obtain

$$AU := 2e^{-i\beta}(P_- - J - cl*)(e^{i\beta}U) = -2e^{-i\beta}(P_- - J - cl*)\xi := g.$$

In addition to the operator R given above we define

$$SU = \text{Im}(e^{-i\beta}(J - iK)(e^{i\beta}U)),$$

$$C_1U = \text{Re}(e^{-i\beta}cl * (e^{i\beta}U)),$$

$$C_2U = \text{Im}(e^{-i\beta}cl * (e^{i\beta}U)),$$

$$J_1U = \text{Re}(2e^{-i\beta}J(e^{i\beta}U)),$$

and

$$J_2U = \text{Im}(2e^{-i\beta}J(e^{i\beta}U)).$$

A straightforward calculation shows that C_1, C_2, J_1 , and J_2 are Fredholm integral operators (integration w.r.t. ϕ) with (continuous) kernels

$$C_1(\theta, \phi) = \frac{\cos(\beta(\theta) - \beta(\phi)) - \rho^{-2} \cos(\beta(\theta) - \beta(\phi) - (\theta + \phi))}{1 + \rho^{-4} - 2\rho^{-2} \cos(\theta + \phi)},$$

$$C_2(\theta, \phi) = -\frac{\sin(\beta(\theta) - \beta(\phi)) - \rho^{-2} \sin(\beta(\theta) - \beta(\phi) - (\theta + \phi))}{1 + \rho^{-4} - 2\rho^{-2} \cos(\theta + \phi)},$$

$$J_1(\theta, \phi) = \frac{1}{\pi} \cos(\beta(\phi) - \beta(\theta)),$$

$$J_2(\theta, \phi) = \frac{1}{\pi} \sin(\beta(\phi) - \beta(\theta)),$$

and are therefore compact operators. For S we obtain the kernel

$$S(\theta, \phi) = -\frac{1}{2\pi} \frac{\cos(\beta(\theta) - \beta(\phi) - (\theta - \phi)/2)}{\sin((\theta - \phi)/2)},$$

so the integral must be taken in the principal value sense and S is not compact. We now expand A using $P_- = \frac{1}{2}(I - iK + J)$ and the above definitions to obtain

$$AU = (I + R_e)U + iS_eU,$$

where

$$R_e = R - 2C_1 - J_1,$$

and

$$S_e = S - 2C_2 - J_2.$$

If $g = g_1 + ig_2$, U real implies

$$(I + R_e)U = g_1.$$

The operator R_e is compact and our treatment of a discrete version of this equation will be similar to that described above when D is the disk.

The normalization on $w = f(z)$ that $f(0) = 0$ can be written as

$$0 = A_0 + \sum_{m=1}^{\infty} A_m T_m(0) = a_0 + 2 \sum_{k=1}^{\infty} (-1)^k \rho^{-2k} a_{2k}. \tag{2}$$

since $T_{2k}(0) = 2(-1)^k$, $T_{2k-1}(0) = 0$, and $A_m = \rho^{-m} a_m$ for $m \geq 0$.

3.3. Cross

The other case that we consider explicitly is a “cross-shaped” region bounded by the curve C_ρ which is the image of $|\zeta| = \rho$ under the map $z = \psi(\zeta) = \sqrt{\zeta^2 + 1/\zeta^2}$. We note that if $\psi_0(\zeta) = \zeta + 1/\zeta$ is the map used for the ellipse then $\psi(\zeta) = (\psi_0(\zeta^2))^{1/2}$.

Generating the Faber polynomials for D is less simple here, but, if

$$F_{2m}(z) = 2^{-2m}((z^2 + \sqrt{z^4 - 4})^m + (z^2 - \sqrt{z^4 - 4})^m),$$

then

$$F_{2m}(\psi(\zeta)) = \zeta^{2m} + \zeta^{-2m},$$

and $F_{2m}(z)$, $m \geq 0$, are degree $2m$ Faber polynomials for D by Proposition 2. These will suffice to generate our algorithm for this domain. In fact by Proposition 1, f defined on C_ρ extends into D analytically if and only if

$$0 = \int_{C_\rho} f(z)F_{2m}(z) dz = \int_{|\zeta|=\rho} \frac{f(\zeta)}{\psi(\zeta)}(\zeta^{2m} + \zeta^{-2m})(\zeta^2 - \zeta^{-2}) d\zeta/\zeta \tag{3}$$

and

$$0 = \int_{C_\rho} f(z)zF_{2m}(z) dz = \int_{|\zeta|=\rho} f(\zeta)(\zeta^{2m} + \zeta^{-2m})(\zeta^2 - \zeta^{-2}) d\zeta/\zeta \tag{4}$$

for $m \geq 1$. If we let

$$f(\theta) = \sum_{m=-\infty}^{\infty} a_m e^{im\theta},$$

and

$$(f/\psi)(\theta) = \sum_{m=-\infty}^{\infty} b_m e^{im\theta},$$

then (3) and (4) are equivalent to

$$b_{-2m} = \rho^{-4m} b_{2m}, \tag{5}$$

and

$$a_{-2m} = \rho^{-4m} a_{2m}, \tag{6}$$

for $m \geq 1$, respectively. As Eqs. (1) were the foundation for our equations for the ellipse, (5) and (6) essentially define our method for the cross. These equations are equivalent to

$$\hat{Q}(P_- - cl * -J)f = 0$$

and

$$\hat{Q}(P_- - cl * -J)(f/\psi) = 0$$

where \hat{Q} is the projection onto functions whose odd order and zeroth Fourier coefficients vanish. We add to these the normalization

$$0 = A_0 + \sum_{m=1}^{\infty} A_m F_m(0).$$

In Appendix A we show that $F_k(0) = 0$ if $k \neq 0 \pmod{4}$, and $F_{4m}(0) = 2(-1)^m$ so that this condition becomes

$$0 = a_0 + 2 \sum_{m=1}^{\infty} (-1)^m \rho^{-4m} a_{4m}. \tag{7}$$

We need an analogous equation (8) involving the b_n 's. For this we note that

$$f/\psi = \zeta^{-1}(1 + \zeta^{-4})^{-1/2} \sum_{m=-\infty}^{\infty} a_m e^{im\theta},$$

and, hence,

$$b_0 = \sum_{m=0}^{\infty} a_{1+4m} B_m \rho^{-4m-1}, \tag{8}$$

since

$$\zeta^{-1}(1 + \zeta^{-4})^{-1/2} = \zeta^{-1} \left(1 + \sum_{m=1}^{\infty} \binom{-\frac{1}{2}}{m} \zeta^{-4m} \right) = \zeta^{-1} \sum_{m=0}^{\infty} B_m \zeta^{-4m}.$$

3.4. Remarks on extensions

Here we discuss some possible extensions of our methods. Generalizations of the cross region to regions with n -fold symmetry would seem to be feasible. If the target region had n elongated legs, one would want the ends of the legs of the computational region to map to the ends of the legs of the target region in order to circumvent the crowding. However, this is equivalent to fixing n boundary points of the conformal map, and this cannot be done for $n > 3$ unless the target region itself possesses a sufficient amount of symmetry. Thus, the case $n = 3$ is particularly interesting. First, note that $\psi_0(\zeta) = \zeta + 1/\zeta + 2$ maps $|\zeta| > 1$ to the exterior of the line segment, $[0, 4]$. Then our symmetric 3-fold region is bounded by the curve C_ρ which is the image of $|\zeta| = \rho > 1$ under the map $z = \psi(\zeta) = (\psi_0(\zeta^3))^{1/3}$.

By Proposition 2, the Faber polynomials of degree $3m$ are

$$F_{3m}(z) = 2^{-m}((z^3 - 2 + \sqrt{z^6 - 4z^3})^m + (z^3 - 2 - \sqrt{z^6 - 4z^3})^m),$$

since

$$F_{3m}(\psi(\zeta)) = \zeta^{3m} + \zeta^{-3m}.$$

By Proposition 1, these yield analyticity conditions on f of the form

$$a_{-3m} = \rho^{-6m} a_{3m}, \quad b_{-3m} = \rho^{-6m} b_{3m}, \quad c_{-3m} = \rho^{-6m} c_{3m},$$

for $m \geq 1$, where a_k, b_k , and c_k are the Laurent coefficients of $f, f/\psi$, and f/ψ^2 , respectively.

4. Discretization, normalization, and numerical implementation

In this section we use N -point trigonometric interpolation to discretize the linear operator equations for U of Section 3. We show how to implement our two normalization conditions (a) $f(0) = 0$, $f(z(0)) = \gamma(0)$, and (b) 3 boundary points fixed. We discuss (b) only for the ellipse, where 2 end points of the ellipse can be mapped to the ends of a slender region as in Example 5, Fig. 4. Adaptation to the disk and the cross, Example 8, Fig. 6, is obvious. An additional condition is

needed for the cross. The auxiliary conditions perturb the eigenvalue distribution of our discrete systems in a well-known way. In each case we use the conjugate gradient method to solve the normal equations. Since the eigenvalues are well-grouped around 1, the conjugate gradient method converges superlinearly. At the end of this section, we discuss the evaluation of the maps.

4.1. Disk

With the normalization $f(0) = 0$, the discrete version of the analyticity conditions from Section 3.1 become

$$\hat{a}_m = 0, \quad m = 0, -1, \dots, -N/2 + 1.$$

With $\frac{1}{N}F\mathbf{h} = \mathbf{a} = (\hat{a}_0, \dots, \hat{a}_{N/2}, \hat{a}_{-N/2+1}, \dots, \hat{a}_{-1})^T$, $E = \text{diag}_k(e^{i\beta(\theta_k)})$, $\mathbf{h} = \xi + E\mathbf{u}$, I_1 and I_2 as in Section 2, $P := (I_1, I_2)$, $C := PFE$, and $\mathbf{c} := -PF\xi$, the discrete analyticity conditions lead to a matrix equation for the unknown $\mathbf{u} = (u_0, \dots, u_{N-1})^T$,

$$C\mathbf{u} = -(I_1 I_2)F\xi =: \mathbf{c}.$$

This is a system of $N/2$ complex equation in N real unknowns (of numerical rank $N - 1$). To fix the boundary point $f(1) = \gamma(0)$, we want $s_0 = 0$ and hence $u_0 = 0$. This condition can be expressed as $u_0 = \mathbf{e}_1^T \mathbf{u} = 0$, where \mathbf{e}_i is the i th standard basis vector for R^N . The full-rank system may now be written as

$$\begin{pmatrix} C \\ \frac{1}{2}\mathbf{e}_1^T \end{pmatrix} \mathbf{u} = \begin{pmatrix} \mathbf{c} \\ 0 \end{pmatrix}.$$

Multiplying by $(\frac{2}{N}C^H \mathbf{e}_1)$ and using \mathbf{u} real, we arrive at the “normal equations”,

$$(I_N + R_N + Q)\mathbf{u} = \mathbf{r}, \tag{9}$$

where

$$I_N + R_N := \frac{2}{N} \text{Re}(C^H C) = \frac{2}{N} \text{Re} \left(E^H F^H \begin{pmatrix} I_1 & 0 \\ 0 & I_2 \end{pmatrix} FE \right)$$

$$Q := \frac{1}{2} \mathbf{e}_1 \mathbf{e}_1^T$$

$$\mathbf{r} := -\frac{2}{N} \text{Re}(C^H \mathbf{c}) = -\frac{2}{N} \text{Re} \left(E^H F^H \begin{pmatrix} I_1 & 0 \\ 0 & I_2 \end{pmatrix} F\xi \right).$$

The definition of R_N as an operator is given by $R_N U := \text{Re}(e^{-i\beta}(J_N - iK_N)e^{i\beta})U$, which is the discretization of R by N -point trigonometric interpolation.

The system (9) now contains the normalization condition $u_0 = 0$ and has full rank numerically. We solve (9) by the conjugate gradient method. This amounts to a slight modification of Fornberg’s original method [14] where the Gauss doubling of the DFT is used to derive a system of $N/2$ unknowns for the u_{2i} ’s. The eigenvalue distribution of R compact and R_N is studied in [14, 26, 27, 30, 11]. In [26], it is shown that -1 is a simple eigenvalue of R and the other eigenvalues occur in pairs $\pm\mu$ with $0 < |\mu| < 1$. The eigenvalues of R_N inherit this structure and so $I_N + R_N$ is symmetric, positive semidefinite with eigenvalues well-grouped around 1. The addition of the

low rank matrix Q perturbs the eigenvalues in a well-known way (see e.g. [16, Theorem 8.1.5, p. 412]) so that $I_N + R_N + Q$ is symmetric, positive definite with eigenvalues remaining well-grouped around 1. Therefore, the conjugate gradient method applied to (9) converges superlinearly and the matrix–vector multiplication costs $O(N \log N)$. In [11] a more detailed discussion of these observations is given. Addition of the normalization term $\frac{1}{2}e_1e_1^T$ is generally necessary. For instance, the method converged for ellipses of $\alpha = 0.8$ and 0.6 without the normalization term, but did not converge for $\alpha = 0.4$. With the normalization term, the method converged in all these cases.

The Newton update at the k th Newton step in all our cases is given by

$$s_i^{(k+1)} = s_i^{(k)} + u_i^{(k)}, \quad i = 0, 1, \dots, N - 1.$$

4.2. Ellipse

For the ellipse, the discrete version of the analyticity conditions from Section 3.2 become

$$\hat{a}_{-m} = \rho^{-2m}\hat{a}_m, \quad m = 1, \dots, N/2 - 1.$$

Note that the discrete analyticity condition makes no sense for $m = N/2$, since $\hat{a}_{-N/2} = \hat{a}_{N/2}$ by the N –periodicity of the discrete Fourier coefficients. Using $\mathbf{a} = (1/N)F\mathbf{h}$ and $P = (P_e, I_e)$, where P_e and I_e are the $(N/2 - 1) \times N/2$ matrices

$$P_e = - \begin{pmatrix} & & & & 0 & \rho^{-N+2} \\ & & & & \cdot & \\ & & 0 & \rho^{-4} & & \\ 0 & \rho^{-2} & & & & \end{pmatrix}, \quad I_e = \begin{pmatrix} 0 & 1 & & & & \\ & 0 & 1 & & & \\ & & \cdot & & & \\ & & & \cdot & & \\ & & & & \cdot & \\ & & & & & \cdot \\ & & & & & & 0 & 1 \end{pmatrix},$$

the discrete analyticity conditions can be written in matrix form as

$$PF\mathbf{h} = \mathbf{0}.$$

Letting $\mathbf{h} = \xi + E\mathbf{u}$, $C = PFE$, and $\mathbf{c} = -PF\xi$, our linear system for \mathbf{u} can be written as

$$C\mathbf{u} = \mathbf{c}.$$

This is now a system of $N/2 - 1$ complex equations in N real unknowns.

At this point we could discretize $I + R_e$ from 3.2 as the nonsymmetric system

$$I_N + R_{e,N} = \frac{2}{N} \operatorname{Re} \left(E^H F^H \begin{pmatrix} P \\ 0 \end{pmatrix} FE \right),$$

where $N/2 + 1$ rows of zeros have been added below P to make an $N \times N$ matrix. After adding the normalization conditions, we could solve the normal equations by the conjugate gradient method. This approach, however, requires 2 FFTs more than the approach that we take next and does not change the convergence rate of the conjugate gradient method.

As in the case of the disk, our normalization conditions can be expressed in the form $\mathbf{q}^T \mathbf{u} = \mathbf{d}$ where \mathbf{q} and \mathbf{d} will be given below. These equations can then be added to the analyticity conditions to get a system of essentially $N + 1$ real conditions for N real unknowns,

$$\begin{pmatrix} C \\ \mathbf{q}^T \end{pmatrix} \mathbf{u} = \begin{pmatrix} \mathbf{c} \\ \mathbf{d} \end{pmatrix}.$$

We will again solve the “normal equations” for \mathbf{u} real,

$$\left(\frac{2}{N} \operatorname{Re}(C^H C) + Q \right) \mathbf{u} = \mathbf{r},$$

where Q and \mathbf{r} are given below. $\frac{2}{N} \operatorname{Re}(C^H C) = \frac{2}{N} \operatorname{Re}(E^H F^H P^T P F E)$ is easily seen to be symmetric, positive semidefinite. In our examples, we find its numerical rank to be $\approx N - 3$. The matrix–vector multiplication costs $O(N \log N)$.

We now discuss the normalization conditions:

(a) $f(0) = 0, f(z(0))$ fixed. For $f(0) = 0$ we need a truncated version of (2). This takes the form

$$\hat{a}_0 + 2 \sum_{k=1}^{N/2-1} (-1)^k \rho^{-2k} \hat{a}_{2k} = 0$$

and can be written $\mathbf{n}^T \mathbf{a} = 0$, where the N vector $\mathbf{n}^T := (1, 0, -2\rho^{-2}, 0, 2\rho^{-4}, \dots)$. With

$$\zeta^T := \mathbf{n}^T F E$$

and

$$\mathbf{d} := \begin{pmatrix} \mathbf{n}^T F \xi \\ 0 \end{pmatrix},$$

we have

$$\mathbf{q}^T := \begin{pmatrix} \zeta^T \\ \mathbf{e}_1^T \end{pmatrix},$$

$$Q := \frac{2}{N} \operatorname{Re}(\bar{\zeta} \zeta^T) + \mathbf{e}_1 \mathbf{e}_1^T,$$

and

$$\mathbf{r} := -\frac{2}{N} \operatorname{Re}(E^H F^H P^T P F \xi) - \frac{2}{N} \operatorname{Re}(\bar{\mathbf{q}} \mathbf{d}).$$

We now can clarify the effect of both normalization conditions on the eigenvalue distribution of our matrices. Letting $\zeta_j = \eta_j + i\mu_j, \eta_j, \mu_j$ real, and $\eta = (\eta_0, \eta_1, \dots, \eta_{N-1})^T, \mu = (\mu_0, \mu_1, \dots, \mu_{N-1})^T$, we have

$$\operatorname{Re}(\bar{\zeta} \zeta^T) = \eta \eta^T + \mu \mu^T.$$

Then since $\eta\eta^T\eta = \|\eta\|_2^2\eta$ and $\mu\mu^T\mu = \|\mu\|_2^2\mu$, the eigenvalues of $2 \operatorname{Re}(\bar{\zeta}\zeta^T)$ are bounded above by $\|\zeta\|_2^2 = \|\eta\|_2^2 + \|\mu\|_2^2$. Note further that

$$\frac{1}{N}\|\zeta\|_2^2 = \frac{1}{N}\|EF\mathbf{n}\|_2^2 = \|\mathbf{n}\|_2^2 \leq 1 + 4 \sum_{i=1}^{\infty} \rho^{-4i} = 1 + \frac{4}{\rho^4 - 1} = O(1/\alpha),$$

where $\alpha = \alpha_{\text{ellipse}} = (\rho^2 - 1)/(\rho^2 + 1)$ is independent of the α of the target region Ω . Numerical studies of the eigenvalues for our normal system show that the largest eigenvalues are indeed $O(1/\alpha)$ and that the rest of the eigenvalues behave similarly to the disk case with grouping around 1, interlacing, and more smearing away from 1 for the more extreme examples where $\alpha \downarrow 0$ ($\rho \downarrow 1$). Therefore, more conjugate gradient iterations are needed.

(b) *3 boundary points fixed.* We wish to fix the values of $f(\pm(\rho + 1/\rho))$ and $f(i(\rho - 1/\rho))$. This is done by fixing $s_0, s_{N/4}$, and $s_{N/2}$, and requires that $u_0 = u_{N/4} = u_{N/2} = 0$. These conditions are easier to apply than those of (a). We express them as $\mathbf{e}_i^T \mathbf{u} = 0, i = 1, N/4 + 1, N/2 + 1$. Then we just use $\mathbf{q} = (\mathbf{e}_1, \mathbf{e}_{N/4+1}, \mathbf{e}_{N/2+1})$, $\mathbf{Q} = \mathbf{q}\mathbf{q}^T$, and $\mathbf{d} = (0, 0, 0)^T$ above.

4.3. Cross

Let $\mathbf{a} = (1/N)F\mathbf{h}$ and $\mathbf{b} = (1/N)F\Psi\mathbf{h}$, where $\Psi := \text{diag}_k(1/\psi(\rho e^{i\theta_k}))$. The discrete versions of the analyticity conditions (5), (6) are then

$$\hat{a}_{-2m} = \rho^{-4m}\hat{a}_{2m}, \quad \hat{b}_{-2m} = \rho^{-4m}\hat{b}_{2m}, \quad m = 1, \dots, N/4 - 1.$$

With $P = (P_c, I_c)$, where P_c and I_c are the $(N/4 - 1) \times N/2$ matrices

$$P_c = - \begin{pmatrix} 0 & 0 & & & 0 & \rho^{-N+4} & 0 \\ \cdot & \cdot & & & \cdot & & \cdot \\ \cdot & \cdot & & & \cdot & & \cdot \\ \cdot & \cdot & & & \cdot & & \cdot \\ 0 & 0 & & 0 & \rho^{-8} & 0 & 0 \\ 0 & 0 & \rho^{-4} & 0 & & & 0 \end{pmatrix}$$

and

$$I_c = \begin{pmatrix} 0 & 0 & 1 & 0 & & & \\ & & 0 & 1 & 0 & & \\ & & & & \cdot & & \\ & & & & \cdot & & \\ & & & & \cdot & & \\ & & & & & & 0 & 1 & 0 \end{pmatrix},$$

these conditions can be written in matrix form,

$$\begin{pmatrix} PF \\ PF\Psi \end{pmatrix} \mathbf{h} = \mathbf{0}.$$

With

$$\mathbf{h} = \boldsymbol{\xi} + E\mathbf{u}, \quad C = \begin{pmatrix} PF \\ PF\Psi \end{pmatrix} E, \quad \text{and} \quad \mathbf{c} = - \begin{pmatrix} PF \\ PF\Psi \end{pmatrix} \boldsymbol{\xi},$$

we again have

$$C\mathbf{u} = \mathbf{c},$$

a system of $N/2 - 2$ complex equations in N real unknowns. Since we can fix one boundary point, we expect the rank of $\text{Re}(C^H C)$ to be $N - 5$. We therefore need 5 more (real) equations: 3 normalization conditions and 2 additional conditions relating the a_k 's and the b_k 's. We consider here only the normalization (a) $f(0) = 0$ and $f(z(0))$ fixed. To impose $f(0) = 0$ we truncate (7) to get

$$\mathbf{n}^T \mathbf{a} = 0,$$

where $\mathbf{n}^T = (1, 0, 0, 0, -2\rho^{-4}, 0, \dots)$. The 2 additional conditions are truncations of (8) which, using $b_0 = (1/N)\mathbf{e}_1^T F\Psi F^H \mathbf{a}$, can be written as

$$\mathbf{m}^T \mathbf{a} = 0,$$

where

$$\mathbf{m}^T = \frac{1}{N} \mathbf{e}_1^T F\Psi F^H - (0, \rho^{-1}, 0, 0, 0, B_1 \rho^{-5}, \dots).$$

The complete set of $N + 1$ real equations of rank N for \mathbf{u} is then

$$\begin{pmatrix} C \\ \mathbf{q}^T \end{pmatrix} \mathbf{u} = \begin{pmatrix} \mathbf{c} \\ \mathbf{d} \end{pmatrix},$$

where

$$\boldsymbol{\zeta}^T = \mathbf{n}^T F E,$$

$$\boldsymbol{\chi}^T = \mathbf{m}^T F E,$$

$$\mathbf{q}^T = \begin{pmatrix} \boldsymbol{\zeta}^T \\ \boldsymbol{\chi}^T \\ \mathbf{e}_1^T \end{pmatrix},$$

and

$$\mathbf{d} = - \begin{pmatrix} \mathbf{n}^T F \boldsymbol{\xi} \\ \mathbf{m}^T F \boldsymbol{\xi} \\ 0 \end{pmatrix}.$$

Our normal equations are again

$$\left(\frac{2}{N} \text{Re}(C^H C) + Q \right) \mathbf{u} = \mathbf{r},$$

where

$$\frac{2}{N} \operatorname{Re}(C^H C) := \frac{2}{N} \operatorname{Re}(E^H F^H P^T P F E + E^H \Psi^H F^H P^T P F \Psi E),$$

$$Q := \frac{2}{N} \operatorname{Re}(\bar{\zeta} \zeta^T + \bar{\chi} \chi^T) + e_1 e_1^T,$$

and

$$r := -\frac{2}{N} \operatorname{Re}(E^H F^H P^T P F \xi + E^H \Psi^H F^H P^T P F \Psi \xi) - \frac{2}{N} \operatorname{Re}(\bar{\zeta} n^T F \xi + \bar{\chi} m^T F \xi).$$

The factor of $2/N$ in the matrix $(2/N) \operatorname{Re}(C^H C)$ normalizes the eigenvalues to be grouped around 1. As in the ellipse case, a calculation, given in Appendix B, shows that the largest eigenvalues are $O(1/\alpha^2)$, $\alpha \downarrow 0$. Our numerical studies show behavior of the eigenvalues similar to the disk and ellipse cases, but with somewhat poorer grouping around 1 and a resulting increase in the number of conjugate gradient iterations.

Remark. For the disk, ellipse, and cross case, we choose $N = 2^M$. However, for the discretization of the 3-fold case in Section 3.4, it is expedient to choose $N = 3 \cdot 2^M$.

4.4. Evaluation of the map

Evaluating the maps for the ellipse or the cross in the interior of the region requires some caution. Let \tilde{a}_k , $k = -N/2 + 1, \dots, -1, 0, 1, \dots, N/2$ be the discrete Laurent coefficients of the approximate map \tilde{f} . Then

$$\tilde{f}(\psi(\rho e^{i\theta})) = \sum_{k=-N/2+1}^{N/2} \tilde{a}_k e^{ik\theta}.$$

To evaluate \tilde{f} in annulus $r e^{i\theta}$, $1 \leq r \leq \rho$ let $\tilde{r} = r/\rho$. Then $1/\rho \leq \tilde{r} \leq 1$ and

$$\tilde{f}(\psi(r e^{i\theta})) = \sum_{k=-N/2+1}^{N/2} \tilde{a}_k \tilde{r}^k e^{ik\theta}.$$

However, we cannot use this to obtain good numerical results, since for $\tilde{r} < 1, k < 0, \tilde{r}^k \rightarrow \infty$. If we had the exact a_k 's then $a_k \tilde{r}^k \rightarrow 0, k < 0$. However, the \tilde{a}_k are only known to the level of the residual error and hence do not decay rapidly enough. That is, $\tilde{a}_k \tilde{r}^k$ can be very large for k near $-N/2$ when ρ and N are large. To get even marginally reasonable looking graphics the finite Laurent series must be truncated further. Even in such cases the images of inner concentric circles may look poor; see [6, Figs. 1, 5, and 7, α large].

To correct this problem for the ellipse we use the relations between the Laurent coefficient, $\tilde{a}_{-k} \approx \rho^{-2k} \tilde{a}_k$ and instead evaluate

$$\tilde{f}(\psi(r e^{i\theta})) = \tilde{a}_0 + \sum_{k=1}^{N/2} \tilde{a}_k \tilde{r}^k e^{ik\theta} + \sum_{k=1}^{N/2-1} \tilde{a}_k (\tilde{r} \rho^2)^{-k} e^{-ik\theta}.$$

Then $\rho \leq \tilde{r}\rho^2 \leq \rho^2$ and the above problems are avoided. Images of $\tilde{f}(\psi(re^{i\theta}))$ for evenly distributed θ_j 's and fixed \tilde{r} may be computed using the FFT. Images of other points are computed using Horner's rule.

We use a similar procedure for the cross. If

$$g(\zeta) = \sum_{k=-\infty}^{\infty} c_k \zeta^k,$$

we denote the even and odd parts of the series by

$$g_e(\zeta) = \sum_{j=-\infty}^{\infty} c_{2j} \zeta^{2j}$$

and

$$g_o(\zeta) = \sum_{j=-\infty}^{\infty} c_{2j+1} \zeta^{2j+1},$$

respectively, and $g = g_e + g_o$. Note that $\psi(\zeta) = \zeta(1 + \zeta^{-4})^{1/2}$ is an odd series, $\psi = \psi_o$. With f , the mapping function, and $f = \psi h$, as above, we have $f_o = \psi h_e$, that is

$$f = f_e + \psi h_e.$$

Then with $\zeta = re^{i\theta}$ and $\tilde{a}_{-2j} = \rho^{-4j} \tilde{a}_{2j}$, we obtain

$$\tilde{f}_e(\psi(re^{i\theta})) = \tilde{a}_0 + \sum_{j=1}^{N/2} \tilde{a}_{2j} \tilde{r}^{2j} e^{i2j\theta} + \sum_{j=1}^{N/2-1} \tilde{a}_{2j} (\tilde{r}\rho^2)^{-2j} e^{-i2j\theta}.$$

Similarly

$$\tilde{h}(\psi(\rho e^{i\theta})) = \sum_{k=-N/2+1}^{N/2} \tilde{b}_k e^{ik\theta},$$

with $\tilde{b}_{-2j} = \rho^{-4j} \tilde{b}_{2j}$ gives

$$\tilde{h}_e(\psi(re^{i\theta})) = \tilde{b}_0 + \sum_{j=1}^{N/2} \tilde{b}_{2j} \tilde{r}^{2j} e^{i2j\theta} + \sum_{j=1}^{N/2-1} \tilde{b}_{2j} (\tilde{r}\rho^2)^{-2j} e^{-i2j\theta}.$$

Combining the above expansions, we may evaluate

$$\tilde{f}(\psi(re^{i\theta})) = \tilde{f}_e(\psi(re^{i\theta})) + \psi(re^{i\theta}) \tilde{h}_e(\psi(re^{i\theta}))$$

for fixed r and evenly distributed θ_j 's using FFT's. Note that even though the \tilde{a}_{2j+1} 's and \tilde{b}_{2j+1} 's could be computed, we do not have the fundamental relations (5) and (6) among the odd indexed coefficients needed for a stable numerical evaluation of the series.

5. Numerical examples

We have tested our methods on a variety of regions exhibited below and found that the ellipse and cross methods work well for regions with elongated sections with $\alpha = 0.1$ or smaller using moderate values of N . This is much better than what is possible with the disk as a computational domain. Our methods for the disk and the ellipse are revisions of the methods [14, 6] and behave in a similar fashion. Our computations were done in double precision on an IBM ES 9000.

Before we discuss the examples, let us give some more programming details. As noted above, we use the radix-2 complex FFT routine [3, p. 416] for the conjugate gradient iterations and the evaluations of the mapping function. The boundary curves are defined by taking N_s points $\gamma_i, i = 1, \dots, N_s$, along the boundary curve, given generally by certain analytic formulas, and interpolating the points by a periodic cubic spline parametrized by the chordal approximation to the arclength between the successive γ_i 's according to the algorithm in [19]. Thus, the regularity of the approximate boundary curve is different than that of the actual boundary curve in most cases. This does not generally affect the accuracy of the approximate map. The important consideration for the computations is that the γ_i 's be distributed with enough density that the derivatives of the the spline yield sufficiently accurate values of the tangent angles for the matrix E above. We take $N_s = 1000$ for the ellipse and disk methods and $N_s = 2000$ for the cross method. Then the spline curves fit the boundary to an accuracy of 10^{-6} or less.

For the ellipse, α is the minor-to-major axis ratio, $\alpha_{\text{ell}} = |\psi(\rho i)/\psi(\rho)|$ where $\psi(\zeta) = \zeta + 1/\zeta$. For the cross, we use $\alpha_{\text{cross}} = |\psi(\rho e^{i\pi/4})/\psi(\rho)|$ where $\psi(\zeta) = \sqrt{\zeta^2 + 1}/\zeta^2$. Given an α for a target region, the α 's for the ellipse or cross are chosen, according to the discussion in Section 6, below, to minimize the discretization error. The mesh points are images of Fourier points under the maps $\psi(\zeta)$. For small α they crowd at the ends of the elongated sections of the computational domains, but the crowding for maps to the exterior of slender regions is not severe (see, e.g. [4, Section 3(ii)]) and is not a source of numerical difficulty in the cases considered so far.

The plots of the maps in the figures show the images of 5 concentric circles and 32 or 64 radial lines in the annulus. The image of $|\zeta| = \rho$ is plotted using $2N$ points and the images of the curves with $1 \leq |\zeta| \leq \rho$ are plotted using N points and employing the formulas developed at the end of Section 4, above.

To monitor the outer Newton iterations, we compute the successive iteration error $\max_i |s_i^{(k+1)} - s_i^{(k)}|$ at the mesh points $\theta_i = 1, \dots, N$. The discretization error is monitored by the residual error,

$$\max_{k \leq 0} |a_{-k}|,$$

for the disk,

$$\max \left(\max_k |a_{-k} - \rho^{-2k} a_k|, |\mathbf{n}^T \mathbf{a}| \right),$$

for the ellipse, and

$$\max \left(\max_k |a_{-2k} - \rho^{-4k} a_{2k}|, \max_k |b_{-2k} - \rho^{-4k} b_{2k}|, |\mathbf{n}^T \mathbf{a}|, |\mathbf{m}^T \mathbf{a}| \right),$$

for the cross. In cases where the exact map is known, the residual error is a good indicator of the exact discretization error. Quadratic convergence is observed, but may degrade for extreme regions.

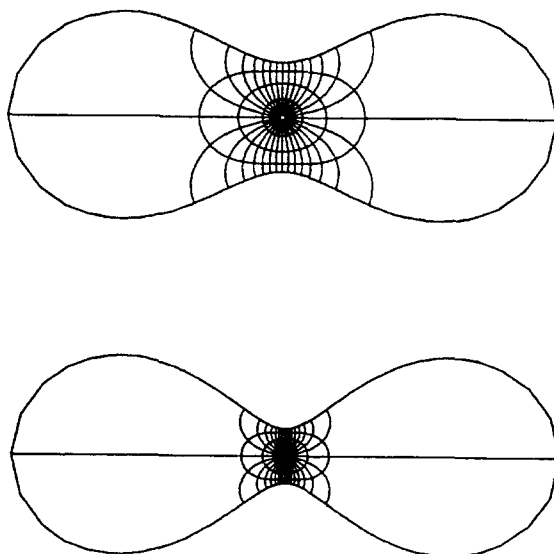


Fig. 2. Cassini ovals with disk map, $\alpha = 0.2, 0.1$, and $N = 256, 1024$, respectively.

Table 1
Cassini ovals with the disk map

α	N	Residual	CPU seconds
0.2	128	$0.11 \cdot 10^{-2}$	1.5
0.2	256	$0.62 \cdot 10^{-4}$	2.3
0.1	256	$0.39 \cdot 10^{-2}$	2.1
0.1	512	$0.32 \cdot 10^{-3}$	7.3
0.1	1024	$0.15 \cdot 10^{-4}$	9.8

The successive iteration error can usually be iterated to 0 ($\approx 10^{-15}$ in double precision), but the convergence rate may slow to linear once the level of discretization error has been reached; see [28]. For our initial guess, we use $S_i^{(0)}$ proportional to $S(\theta_i)$ for the map, $\psi(\rho e^{i\theta_i})$.

Next, we discuss our examples.

Example 1 (*Disk to Cassini ovals, Fig. 2*). This example is discussed in [4, 14]. Utilizing Proposition 3, above, the exact map is given by $f(z) = (k(r^2 z^2)/k(r^2))^{1/2}$ for $|z| \leq 1$ where $k(z) = z/(1-z)$. In this case $\alpha = \sqrt{(1-r^2)/(1+r^2)}$ and the maximum derivative is given by $f'(1) = 1/(2\alpha^2) + 1/2$, so this is a case of algebraic crowding. Residual errors and timings in CPU seconds are given in Table 1.

Example 2 (*Disk to arctanh regions, Fig. 1, top map*). This example is discussed in [4, 10]. The exact map is given by $f(z) = k(rz)/k(r)$ for $|z| \leq 1$ where $k(z) = \text{arctanh}(z) = \frac{1}{2} \log((1-z)/(1+z))$. In this case $\alpha = |f(i)|$, and $r \sim 1 - e^{-\pi/2\alpha}$ and the maximum derivative $|f'(1)| \sim \frac{1}{2} e^{\pi/2\alpha}$ as $\alpha \downarrow 0$.

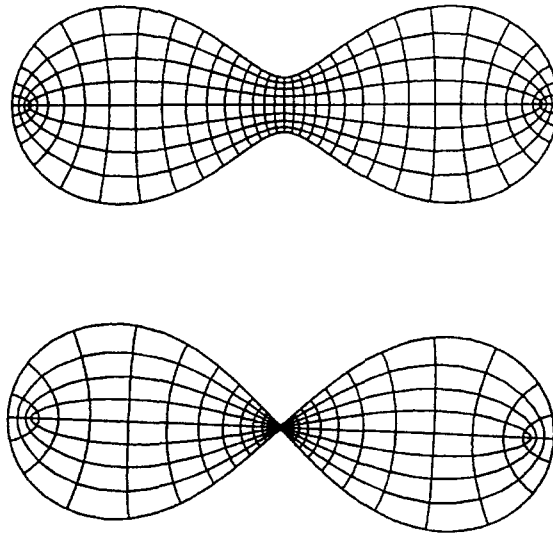


Fig. 3. Cassini ovals with ellipse map, $\alpha = 0.1, 0.01$, and $N = 128, 256$, respectively.

Table 2
Cassini ovals with the ellipse map

α_{Cass}	α_{ell}	N	Residual	CPU sec
0.1	0.3	64	$0.14 \cdot 10^{-5}$	1.3
0.1	0.3	128	$0.10 \cdot 10^{-9}$	1.5
0.01	0.2	128	$0.12 \cdot 10^{-6}$	2.5
0.01	0.2	256	$0.21 \cdot 10^{-9}$	4.6

This map provides a simple example of exponential crowding. The results of our computations are comparable to the results reported for Wegmann's method in [4].

Example 3 (*Ellipse to Cassini ovals, Fig. 3*). Here we apply the ellipse map to the regions in Example 1. Residual errors and timings in CPU seconds are given in Table 2. α_{Cass} denotes α for the Cassini ovals and α_{ell} denotes α for the ellipse. By comparing Table 1 and Table 2, the improvements in efficiency and accuracy of the ellipse map over the disk map can be easily seen.

Example 4 (*Ellipse to arctanh regions, Fig. 1, second map from top*). Here we apply the ellipse map to the regions in Example 2. The results of our computations are similar to those reported in [6].

Example 5 (*Ellipse to a spline region with 3 boundary points fixed, Fig. 4*). In this example the boundary of the region is given by selecting several points placed in the plane and interpolating them with our periodic cubic spline routine. This provides a type of example which occurs in

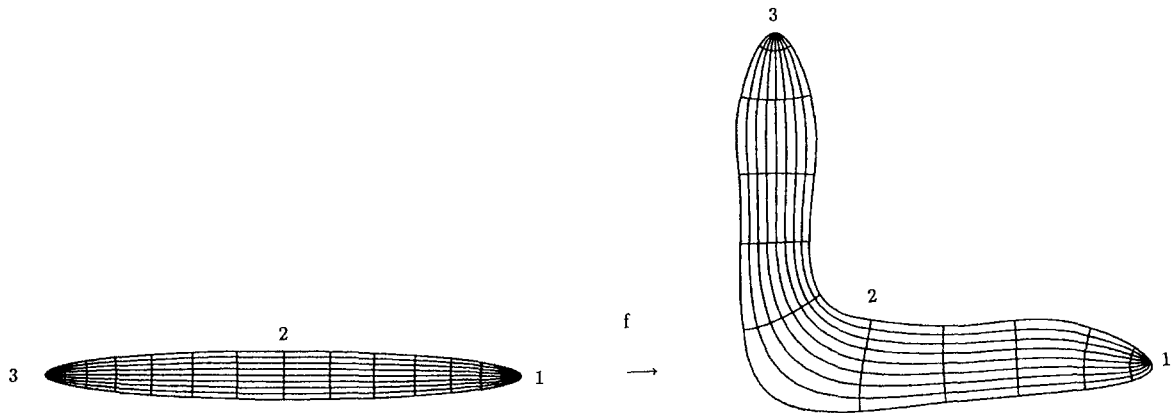


Fig. 4. Spline boundary with ellipse map, $\alpha_{\text{ellipse}} = 0.1$ and $N = 256$ and boundary points 1, 2, and 3 fixed.

Table 3
Spline curve, 3 boundary points fixed, $\alpha_{\text{ell}} = 0.1$

N	Newt it	suc it er	Residual	CPU sec
128	6	$0.28 \cdot 10^{-4}$	$0.17 \cdot 10^{-3}$	1.9
256	6	$0.17 \cdot 10^{-6}$	$0.15 \cdot 10^{-4}$	3.5
512	7	$0.62 \cdot 10^{-9}$	$0.56 \cdot 10^{-9}$	7.6

Table 4
4-leaf Koebe regions with the cross map

α_{Koebe}	α_{cross}	N	Residual	CPU sec
0.2	0.4	128	$0.22 \cdot 10^{-5}$	3.9
0.2	0.4	256	$0.51 \cdot 10^{-10}$	14.3
0.01	0.2	256	$0.29 \cdot 10^{-3}$	7.6
0.01	0.2	512	$0.12 \cdot 10^{-5}$	15.3

practice. Results are given in Table 3, where we have also listed the number of Newton iterations (Newt. it.) and the final error between successive iterates (suc. it. er.).

Example 6 (Cross to 4-leaf Koebe regions, Fig. 1, bottom map). In this example the boundary of the region is given by $f(z) = (k(r^4 z^4)/k(r^4))^{1/4}$ for $|z| = 1$, where $k(z) = z/(1 - z)^2$ is the Koebe function. Here $\alpha_{\text{Koebe}} = \sqrt{(1 - r^4)/(1 + r^4)}$, so r may readily be found in terms of α . In Fig. 1, bottom map, $\alpha_{\text{cross}} = 0.6, \alpha_{\text{Koebe}} = 0.4, N = 256$, and the residual = $0.11 \cdot 10^{-14}$. Results for some other regions are given in Table 4. The times for this method are greater than the disk and ellipse methods for the same values of N . The disk and ellipse methods require 2 FFT's per conjugate gradient iteration, whereas the cross method requires 5 FFT's per iteration and generally several more conjugate gradient iterations in the early Newton steps. Note that this family of regions provides another example of

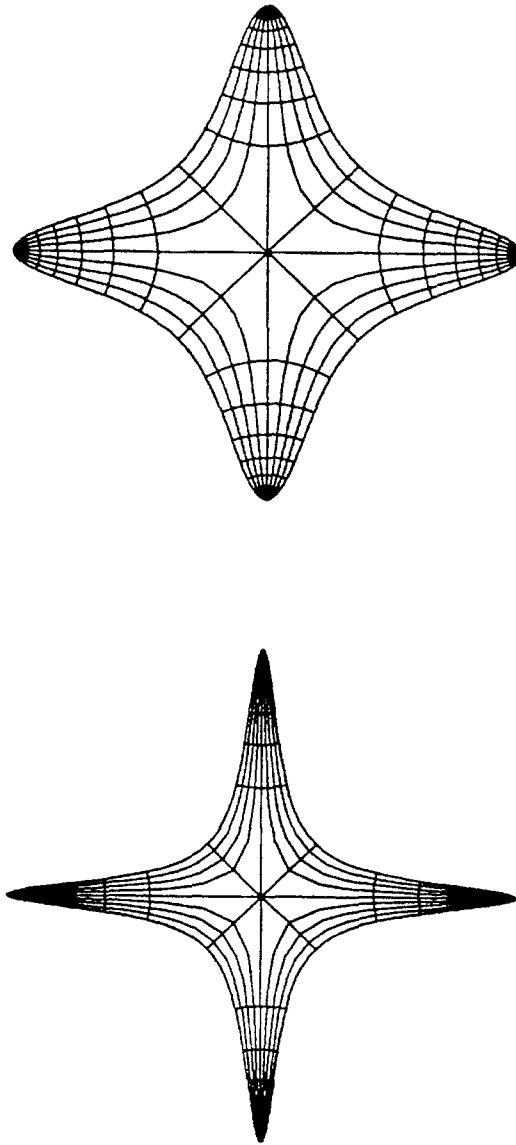


Fig. 5. 4-leaf arctanh region with cross map, $\alpha = 0.41, 0.29$, and $N = 256, 256$, respectively.

algebraic crowding for the disk map. Arbitrary degrees of algebraic crowding and regions with an arbitrary number of leaves may be constructed using the Koebe function and Proposition 3.

Example 7 (*Cross to 4-leaf arctanh regions, Fig. 5*). In this example the boundary of the region is given by $f(z) = (k(r^2 z^2)/k(r^2))^{1/2}$ for $|z| = 1$, where $k(z) = \operatorname{arctanh}(z)$. Here $\alpha_{4\text{arc}} = |f(e^{i\pi/4})|$. Residual errors and timings in CPU seconds are given in Table 5 where $\alpha_{4\text{arc}} = 0.41, 0.29$ ($r = 0.9999, 0.99999999$, respectively).

Table 5
4-leaf arctanh regions with the cross map

α_{4arc}	α_{cross}	N	Residual	CPU sec
0.41	0.5	128	$0.48 \cdot 10^{-8}$	4.2
0.41	0.5	256	$0.57 \cdot 10^{-15}$	8.9
0.29	0.3	256	$0.47 \cdot 10^{-6}$	14.3
0.29	0.3	512	$0.32 \cdot 10^{-11}$	28.9

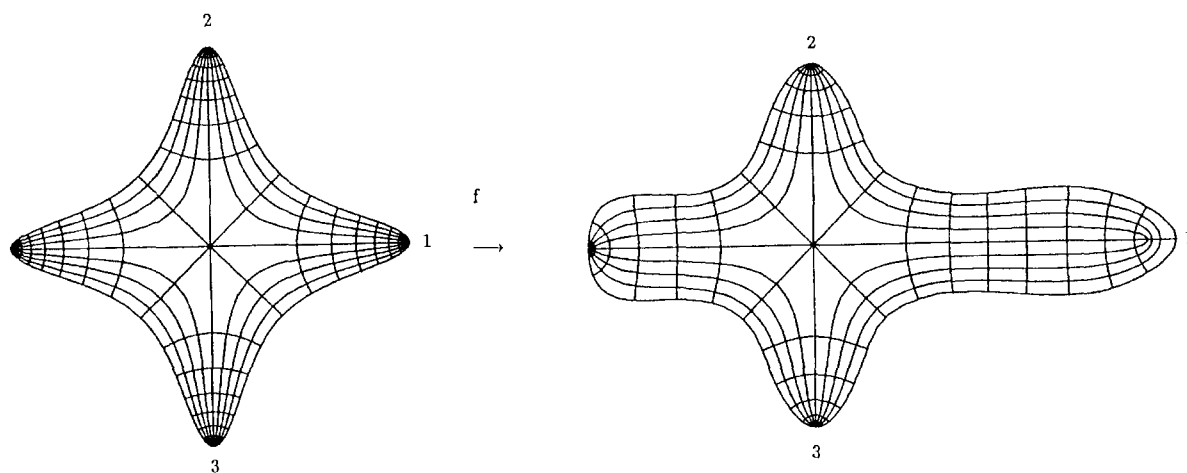


Fig. 6. Spline boundary with cross map, $\alpha_{cross} = 0.5$ and $N = 256$ and boundary points 1, 2, and 3 fixed.

Example 8 (Cross to spline region with 3 boundary points fixed, Fig. 6, $\alpha_{cross} = 0.5, N = 256$, and the residual error $= 0.13 \cdot 10^{-14}$).

6. Accuracy

We will address two questions regarding the accuracy of our methods. They are both concerned with the number of terms used in a Faber (or Fourier) series.

First, we consider a map f from an ellipse to a target domain Ω . The ellipse has minor-to-major axis ratio $\alpha = (\rho^2 - 1)/(\rho^2 + 1)$, and we will want to vary ρ , so we denote f by f_ρ . We denote by $S_n(f_\rho)$ the n th partial sum of the Faber series. It is convenient to refer back to the annulus $1 < |\zeta| < \rho$. Suppose f_ρ extends analytically beyond the ellipse and that when the singularities are pulled back to the ζ -plane the singularity nearest $|\zeta| = \rho$ lies on $|\zeta| = R = R_\rho$. Then a result given by Ellacott [13, Corollary 2.2] implies that

$$\|f_\rho - S_n(f_\rho)\|_\infty \leq 2M(\rho/R_\rho)^{n+1}/(1 - \rho/R_\rho),$$

where M is the maximum of $|f_\rho|$ over the image of $|\zeta| = R_\rho$ by the Joukowski map. In general M will be infinite, but if we consider slightly smaller values of $|\zeta|$ it is a fixed number independent of

Table 6
Optimal α for ellipse map to Cassini oval

α_{Cassini}	N	α_{ellipse}	Residual
0.1	64	0.5	$0.21 \cdot 10^{-2}$
0.1	64	0.4	$0.91 \cdot 10^{-5}$
0.1	64	0.3 (optimal)	$0.14 \cdot 10^{-5}$
0.1	64	0.2	$0.13 \cdot 10^{-3}$
0.1	64	0.1	$0.57 \cdot 10^{-2}$
0.1	128	0.5	$0.13 \cdot 10^{-3}$
0.1	128	0.4	$0.11 \cdot 10^{-8}$
0.1	128	0.3 (optimal)	$0.10 \cdot 10^{-9}$
0.1	128	0.2	$0.14 \cdot 10^{-6}$
0.1	128	0.1	$0.12 \cdot 10^{-1}$
0.01	128	0.3	$0.80 \cdot 10^{-2}$
0.01	128	0.2 (optimal)	$0.12 \cdot 10^{-6}$
0.01	128	0.15	$0.16 \cdot 10^{-5}$
0.01	128	0.1	$0.65 \cdot 10^{-4}$
0.01	256	0.3	$0.50 \cdot 10^{-3}$
0.01	256	0.2 (optimal)	$0.21 \cdot 10^{-9}$
0.01	256	0.15	$0.17 \cdot 10^{-8}$
0.01	256	0.1	$0.51 \cdot 10^{-7}$

Table 7
Optimal α estimated by matching derivatives

α_{ell}	$\sim F'_{\text{ell}}(1) $	α_{Cass}	$ F'_{\text{Cass}}(1) $
0.4	12.2		
0.35	22.4		
0.3	53.4	0.1	50.5
0.25	192.3		
0.2	1451.3	0.01	5000.5
0.15	49,872.4		
0.1	$8.27 \cdot 10^7$		

n . The behavior of the error is $O((\rho/R)^{n+1})$, for any number $\rho < R < R_\rho$. In our methods we do not compute $S_n(f_\rho)$ but an approximation based on taking a certain number of Fourier coefficients on $\zeta = \rho e^{i\theta}$. The behavior of the error is similar, as in the case of the disk map [4, 25]. The behavior of the error is best understood in terms of the ratio ρ/R_ρ . In particular, we may ask if there is an optimal value of ρ , and equivalently of α , for a given target domain. Ellacott's estimate suggests that the optimal ρ is the one which minimizes ρ/R_ρ . Wegmann [29] has recently extended his Riemann–Hilbert method for the disk [24, 25] to the ellipse. [29] gives a somewhat different discussion of the accuracy of the approximation to $S(\theta)$ for the ellipse map.

In Table 6 we give some numerical results which approximate the optimal $\alpha = \alpha_{\text{ellipse}}$ for the map to Cassini ovals of $\alpha = \alpha_{\text{Cassini}} = 0.1$ and 0.01. The optimal α are independent of N in each case.

Since the maximum derivative of map from the unit disk to the Cassini oval grows more slowly in $1/\alpha$ than the maximum derivative of the map from the unit disk to the ellipse, one expects that the optimal α for the ellipse map to the Cassini oval should be greater than α_{Cassini} . This is indeed what we find. If the target region is an arctanh region, so that the maximum derivative grows exponentially in $1/\alpha$ like the ellipse, then we would expect $\alpha_{\text{optimal}} \approx \alpha_{\text{arctanh}}$. We have also found this to be the case. When the maps from the unit disk to the target region are known explicitly, choosing the α that matches the maximum derivatives provides a good criterion for the optimal α , as indicated in Table 7. In practice, where the derivatives of the map are not generally known, one could perform a preliminary search with N relatively small to approximate the optimal α and then perform the final calculation of the mapping function with N sufficiently large to yield the desired accuracy. The optimal α does not have to be found with much precision, but if α_{ellipse} is too far from it, the method will fail to converge. The observations in [4] connecting the crowding to the geometric properties of the region are helpful in providing a first guess of the optimal α . Similar ideas can be applied to the cross map.

The second question that we address is whether a criterion can be given for the number of terms required for the derivative of the map to be well approximated. Our target domain is again Ω with boundary curve Γ and T is the length of Γ . We recall the Zemach rule [4, 31], which says that, for the map F from the disk D to Ω , the number of Fourier coefficients required is at least

$$N = N(D) \geq \frac{2\pi}{T} \|F'\|_\infty.$$

The crowding problem may be thought of as arising from large values of F' at points mapping to the ends of the boundary of slender parts of Ω . We note in particular the example $F(z) = z/(c^2 - z^2)$, $c > 1$ for which the above rule gives $N \geq (2\pi/T)(c^2 + 1)/(c^2 - 1)^2$.

In discussing this question for the ellipse it is useful to refer back to the annulus as before and also to introduce a domain obtained by slitting the unit disk along the interval $[-L, L]$ where $L < 1$. This new domain can be mapped onto the annulus by $\zeta = g(z)$, a mapping given explicitly in terms of elliptic functions, obtained from [21, pp. 293–5] with slight modification. The maps we have introduced are described in Fig. 7. We note that Nehari [21, p. 295] gives

$$L = L(\rho) = \frac{2}{\rho} \prod_{n=1}^{\infty} \left(\frac{1 + (1/\rho)^{8n}}{1 + (1/\rho)^{8n-4}} \right)^2.$$

Our method for constructing f is based on finding h . Hence, if Γ is given by $h(\rho e^{i\theta})$, $0 \leq \theta \leq 2\pi$, then $d\sigma/d\theta = \rho|h'(\rho e^{i\theta})|$. Suppose that $N(A) = 2\pi/\Delta\theta$ is the number of equally spaced points that we take on $|\zeta| = \rho$. Then

$$\frac{d\sigma}{d\theta} \approx \frac{\Delta\sigma}{\Delta\theta} \leq \frac{T}{\Delta\theta} = \frac{T}{2\pi/N(A)}$$

implies $N(A) \geq (2\pi\rho/T)\|h'\|_\infty$. Now, since $F(z) = h(g(z))$, $h'(g(z)) = F'(z)/g'(z)$, and the explicit formula

$$|g'(e^{i\delta})| = \frac{\pi\rho}{2K|e^{2i\delta} - L^2|}$$

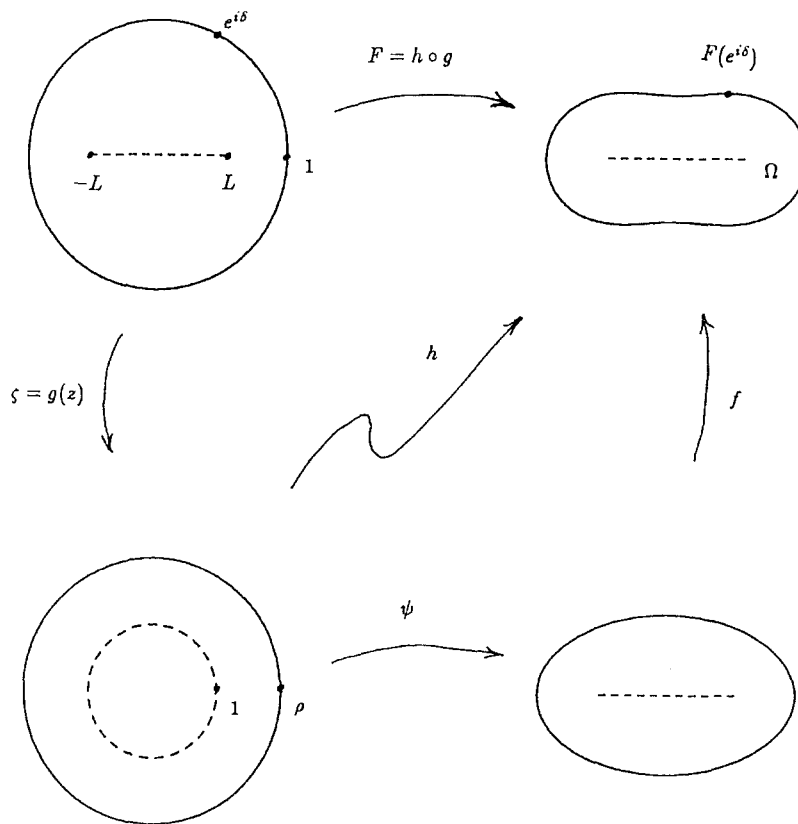


Fig. 7. Illustration for Zemach's rule for the ellipse map.

(where the constant K is given in [21, p. 281]) implies that

$$\|h'\|_\infty = \frac{2K}{\pi\rho} \max_\delta |e^{2i\delta} - L^2| |F'(e^{i\delta})|.$$

One sees that the factor $|e^{2i\delta} - L^2|$ has the possibility of ameliorating the ill effects of large values of $|F'|$. In the particular case of our example $F(z) = z/(c^2 - z^2)$,

$$|e^{2i\delta} - L^2| |F'(e^{i\delta})| = \frac{|e^{2i\delta} - L^2| |c^2 + e^{2i\delta}|}{|c^2 - e^{2i\delta}|^2}.$$

The extreme cases are for $\delta = 0, \pi$, and, in order for this quantity to be bounded when c approaches 1, we need only choose ρ so that $L = 1 - (c - 1)^2$.

A similar analysis can be given for the cross. We write $g_2(z) = \sqrt{\rho g(z^2)}$. A set of maps analogous to those above are depicted in the Fig. 8. We obtain the rule

$$N(A) \geq \frac{4K\rho}{T} \max_\delta |e^{4i\delta} - L^2| |F'(e^{i\delta})|.$$

We omit further details.

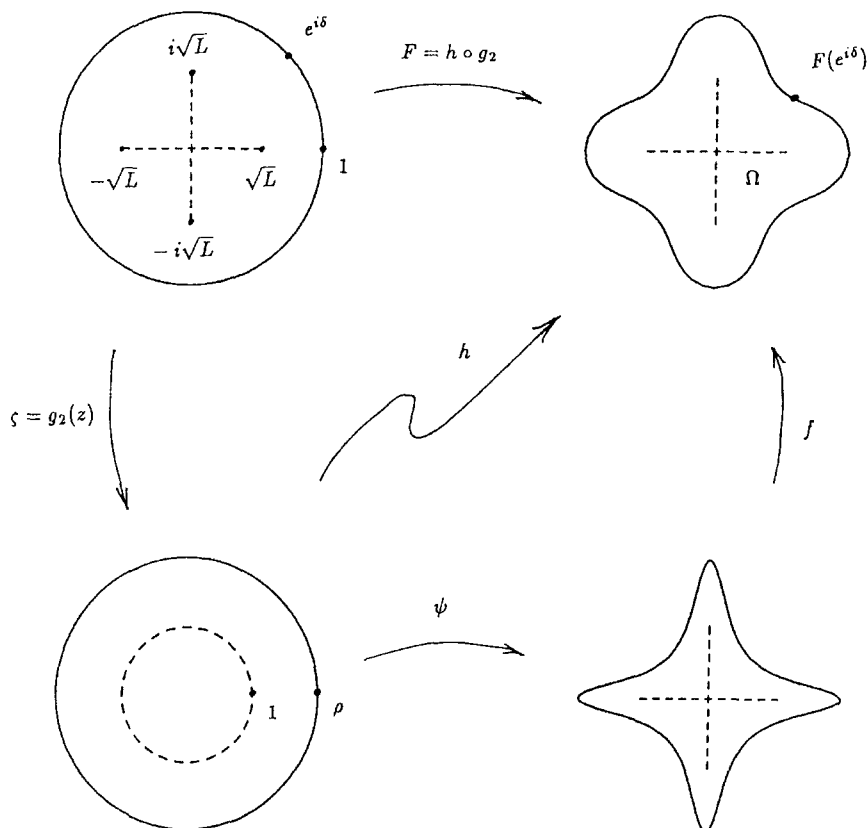


Fig. 8. Illustration for Zemach's rule for the cross map.

As remarked above, these observations suggest a simple procedure for estimating the optimal α if maximum derivative of the map from the unit disk to the target region is known in terms of α . We let F_{ell} be the map from the unit disk to the ellipse and F_{Cass} be the map from the unit disk to the Cassini oval. The maximum derivatives in both cases occur at ± 1 and are given by $|F'_{\text{ell}}(1)| \sim (\alpha^2/2\pi)e^{\pi^2/4\alpha}$ and $|F'_{\text{Cass}}(1)| = 1/2\alpha^2 + \frac{1}{2}$. For a given α_{Cass} , the optimal α is the α_{ell} such that $|F'_{\text{ell}}(1)| = |F'_{\text{Cass}}(1)|$. Some sample derivatives indicating this are given in Table 7; see also Table 6.

Appendix A

We need to derive recursion relations for $F_n(z)$ in the case of the cross. First, the binomial expansion implies that

$$z = \psi(\zeta) = (\zeta^2 + \zeta^{-2})^{1/2} = \zeta + \sum_{k=1}^{\infty} C_k \zeta^{1-4k},$$

where

$$C_k = \binom{\frac{1}{2}}{k} = (-1)^{k-1} 1 \cdot 3 \cdot 5 \cdots (2k - 3) / (2^k k!).$$

The even index polynomials satisfy the simple relation $F_{2m}(z) = \zeta^{2m} + \zeta^{-2m}$, $m = 1, 2, \dots$, but the odd index case is more complex. If the general relations given in [2] are specialized to our situation the relations

$$F_{4m}(z) = F_1(z)F_{4m-1}(z) - \sum_{j=1}^{m-1} C_j F_{4(m-j)}(z) - 4mC_m$$

and

$$F_{4m+k}(z) = F_1(z)F_{4m+k-1}(z) - \sum_{j=1}^{m-1} C_j F_{4(m-j)+k}(z), \quad k = 1, 2, 3$$

follow. These can be used to show, recursively, that $F_m(0) = 0$ if $m \neq 0 \pmod{4}$, and $F_{4m}(0) = 2(-1)^m$.

Appendix B

Note from Section 4.3 that $\|\zeta\|_2^2/N = \|\mathbf{n}\|_2^2$ and $\|\chi\|_2^2/N = \|\mathbf{m}\|_2^2$ and so $\|\mathbf{n}\|_2^2$ and $\|\mathbf{m}\|_2^2$ are eigenvalues of $\bar{\zeta}\zeta^T/N$ and $\bar{\chi}\chi^T/N$, respectively.

Recall that $\mathbf{n}^T = (1, 0, 0, 0, -2\rho^{-4}, 0, 0, 0, -2\rho^{-8}, 0, \dots)$ and so

$$\|\mathbf{n}\|_2^2 \leq 1 + 4 \sum_{j=1}^{\infty} \rho^{-8j} = 1 + \frac{4}{\rho^8 - 1} \sim \frac{1}{\alpha^2}, \quad \alpha \downarrow 0, \quad (\rho \downarrow 1).$$

Recall $\mathbf{m}^T = (1/N)\mathbf{e}_1^T F \Psi F^H - \mathbf{b}^T$ and $\mathbf{b}^T = (0, \rho^{-1}, 0, 0, 0, B_1 \rho^{-5}, 0, \dots)$. Then

$$\|\mathbf{b}\|_2^2 \leq \|\mathbf{b}\|_1^2 \leq \left(\rho^{-1} \sum_{j=0}^{\infty} B_j (-\rho^{-4})^j \right)^2 = \frac{1}{\rho^2(1 - \rho^{-4})} \sim \frac{1}{2\alpha^2}, \quad \alpha \downarrow 0,$$

and

$$\left\| \frac{1}{N} \mathbf{e}_1^T F \Psi F^H \right\|_2^2 = \|\Psi\|_2^2 \leq \left(\max_{\theta} \frac{1}{|\psi(\rho e^{i\theta})|} \right)^2 = \frac{1}{\rho^2(1 - \rho^{-4})} \sim \frac{1}{2\alpha^2}, \quad \alpha \downarrow 0,$$

so

$$\|\mathbf{m}\|_2^2 \leq (\|\Psi\|_2 + \|\mathbf{b}\|_2)^2 \sim \frac{2}{\alpha^2}, \quad \alpha \downarrow 0.$$

Next, note from [16, p. 58], that

$$\|P\|_2 = \|(P_c \ I_c)\|_2 \leq \sqrt{\|(P_c \ I_c)\|_1 \|(P_c \ I_c)\|_{\infty}} \leq \sqrt{2}$$

and so

$$\|P^T P\|_2 \leq \|P\|_2^2 \leq 2.$$

Thus we have that

$$\begin{aligned} \|2\operatorname{Re} C^H C/N + Q\|_2 &\leq 2(\|P\|_2^2 + \|\Psi\|_2^2 \|P\|_2^2 + 2\|\bar{\zeta}\zeta^T\|_2/N + 2\|\bar{\chi}\chi^T\|_2/N) + 1 \\ &\leq 4(1 + \|\Psi\|_2^2) + 2\|n\|_2^2 + 2\|m\|_2^2 + 1 \sim \frac{8}{\alpha^2}, \quad \alpha \downarrow 0. \end{aligned}$$

References

- [1] R.H. Chan, T.K. DeLillo, M.A. Horn, The numerical solution of the biharmonic equation by conformal mapping, *SIAM J. Sci. Comput.*, to appear.
- [2] J.H. Curtis, Faber polynomials and the Faber series, *Amer. Math. Monthly* 78 (1971) 577–596.
- [3] G. Dahlquist, Å. Björck, *Numerical Methods*, Prentice-Hall, Englewood Cliffs, NJ, 1974.
- [4] T.K. DeLillo, The accuracy of numerical conformal mapping methods: a survey of examples and results, *SIAM J. Numer. Anal.* 31 (1994) 788–812.
- [5] T.K. DeLillo, A.R. Elcrat, A comparison of some numerical conformal mapping methods for exterior regions, *SIAM J. Sci. Statist. Comput.* 12 (1991) 399–422.
- [6] T.K. DeLillo, A.R. Elcrat, A Fornberg-like conformal mapping method for slender regions, *J. Comput. Appl. Math.* 46 (1993) 49–64.
- [7] T.K. DeLillo, A.R. Elcrat, K.G. Miller, Constant vorticity Riabouchinsky flows from a variational principle, *ZAMP* 41 (1990) 755–765.
- [8] T.K. DeLillo, M.A. Horn, The numerical solution of the Laplace equation for slender regions, in preparation.
- [9] T.K. DeLillo, M.A. Horn, J.A. Pfaltzgraff, work in progress.
- [10] T.K. DeLillo, J.A. Pfaltzgraff, Extremal distance, harmonic measure and numerical conformal mapping, *J. Comput. Appl. Math.* 46 (1993) 103–113.
- [11] T.K. DeLillo, J.A. Pfaltzgraff, Numerical conformal mapping methods for simply and doubly connected regions, *SIAM J. Sci. Comput.*, to appear.
- [12] T.A. Driscoll, S.A. Vavasis, Numerical conformal mapping using cross-ratios and Delauney triangulation, Cornell Theory Center Technical Report. CTC96TR233 (1996).
- [13] S.W. Ellacott, Computation of Faber series with application to numerical polynomial approximation in the complex plane, *Math. Comput.* 40 (1983) 575–587.
- [14] B. Fornberg, A numerical method for conformal mappings, *SIAM J. Sci. Statist. Comput.* 1 (1980) 386–400.
- [15] D. Gaier, *Konstruktive Methoden der konformen Abbildung*, Springer, Berlin, Göttingen, Heidelberg, 1964.
- [16] G.H. Golub, C.F. Van Loan, *Matrix Computations*, 2nd ed., Johns Hopkins, Baltimore, 1989.
- [17] G.M. Goluzin, *Geometric Theory of Functions of a Complex Variable*, AMS Trans. Math. Monographs, vol. 26, AMS, Providence, RI, 1969.
- [18] P. Henrici, *Applied and Computational Complex Analysis*, vol. III, Wiley, New York, 1986.
- [19] W.D. Hoskins, P.R. King, Periodic cubic spline interpolation using parametric splines, *Algorithm* 73, *Comput. J.* 15 (1972) 282–283.
- [20] L.H. Howell, L.N. Trefethen, A modified Schwarz–Christoffel transformation for elongated regions, *SIAM J. Sci. Statist. Comput.* 11 (1990) 928–949.
- [21] Z. Nehari, *Conformal Mapping*, McGraw-Hill, New York, 1952.
- [22] N. Papamichael, N. Stylianopoulos, On the theory and application of a domain decomposition method for computing conformal modules, *J. Comput. Appl. Math.* 50 (1994) 33–50.
- [23] G. Schober, *Univalent Functions – Selected Topics*, Lecture Notes in Math. vol. 478, Springer, Berlin, 1975.
- [24] R. Wegmann, Ein Iterationsverfahren zur konformen Abbildung, *Numer. Math.* 30 (1978) 453–466; translated as: An iterative method for conformal mapping. in: L.N. Trefethen (Ed.), *Numerical Conformal Mapping*, North-Holland, Amsterdam, 1986; also in *J. Comput. Appl. Math.* 14 (1986) 7–18.
- [25] R. Wegmann, Convergence proofs and error estimates for an iterative method for conformal mapping, *Numer. Math.* 44 (1984) 435–461.
- [26] R. Wegmann, On Fornberg’s numerical method for conformal mapping, *SIAM J. Numer. Anal.* 23 (1986) 1199–1213.

- [27] R. Wegmann, Discrete Riemann–Hilbert problems, interpolation of simply closed curves, and numerical conformal mapping, *J. Comput. Appl. Math.* 23 (1988) 323–352.
- [28] R. Wegmann, Discretized versions of Newton type iterative methods for conformal mapping, *J. Comput. Appl. Math.* 29 (1990) 207–224.
- [29] R. Wegmann, Fast conformal mapping of an ellipse to a simply connected region, *J. Comput. Appl. Math.* 72 (1996) 101–126.
- [30] O. Widlund, On a numerical method for conformal mapping due to Fornberg, unpublished.
- [31] C. Zemach, A conformal map formula for difficult cases, in: L.N. Trefethen (Ed.), *Numerical Conformal Mapping*, North-Holland, Amsterdam, 1986, pp. 207–216.